

NEW FLUORITE INDEX USING ASTER DATA OF GABAL ABU DIYAB AREA, CENTRAL EASTERN DESERT, EGYPT

Mahmoud Hafez^{a,*}, Ibrahim Abu El-Leil^a, Nehal Soliman^b, Mostafa Abu Bakr^a

^a Geology Department, Faculty of Sciences, Al-Azhar University, Nasr City, Cairo, Egypt.

^b Geology Department, National Authority for Remote Sensing and Space Sciences, Cairo, Egypt.

*Corresponding author, Email: mahmoud_hafez@azhar.edu.eg

Received: 09 Sep 2021; Revised: 17 Sep 2021; Accepted: 03 Oct 2021; Published: 01 Dec 2021

ABSTRACT

Remote sensing represents a significant function in the exploration of minerals. Extraction and identification of mineral occurrences in semi-arid to arid regions are some of the remote sensing confirmed uses. The Advanced Spaceborne Thermal Emission and Reflection Radiometer (ASTER) images have been combined with band ratio processing technique for detecting the fluorite mineral occurrences in the area around Gabal Abu Diyab, Central Eastern Desert, Egypt. The proposed band ratio derived from ASTER images Spectra [(b8/b6) * (b5/b3)] can be considered to represent the new Fluorite Index (FI). The USGS Spectral libraries are used to extract the new index and validated it by using the field study. According to the given new Fluorite Index (FI) combined with the field observations, two occurrences of fluorite mineralization at Gabal Homrit Waggat and Gabal Ineiqi have been identified. This study provides the proposed FI as a beneficial tool for fluorite exploration that could be applicable along with Arabian Nubian Shield and similar arid and semi-arid environments.

Keywords: ASTER; Band Ratio; Fluorite Index; FI; Gabal Abu Diyab

1. INTRODUCTION

Since the early 1940s, remote sensing has been used in mineral prospecting, with handheld cameras fixed on plane windows [1]. This technique had been advanced to use the gray shaded color through aerial photos in geological mapping in 1952, however, the more developed space technology of satellite and airborne multispectral and hyperspectral digital imaging systems had been used. Many authors used different satellite images methodologies for the mapping of hydrothermal mineralized zones of the Precambrian rocks in the Arabian-Nubian Shield, e.g., [2-8]. Moreover, the studying of mineral exploration using different image processing techniques such as constrained energy minimization (CEM), principal component analysis (PCA) and band

Available at Egyptian Knowledge Bank (EKB)

rationing had been taken into consideration., e.g., [9-13]. On the other hand, for lithological mapping ASTER data outperforms other sensors as it has more spectral bands that provide a better understanding of the geology of the earth's surface, [14-16]. In this study, we used ASTER imagery and Spectra of USGS spectral libraries for defining the occurrence of fluorite mineralization in the study area. We proposed a new FI that shows a more advanced and suitable tool for prospecting fluorite mineralization. The given results are validated and confirmed by field studies, as well as the metallogenic map is given by [17].

2. STUDY AREA AND GEOLOGICAL SETTING.

The area of study locates around Gabal Abu Diyab, Central Eastern Desert, (Fig.1).
Journal Homepage: <https://absb.journals.ekb>

The area around Gabal Abu Diyab represents a part of the Arabian-Nubian Shield, covered mainly by Precambrian rocks related to ophiolite and island arc assemblage, late and post-orogenic stages, Pan African and Post Pan African orogenic stages respectively. The early Pan African stage comprises the metamorphosed rocks of ophiolite and island arc assemblage-related rocks up to the greenschist facies of highly folded rocks, whereas the ophiolite rocks thrust over the island arc rocks, (Fig. 2). Collided and amalgamated ophiolite and island arc rocks assemblage had been followed by the intrusions of late and Post magmatism, as well as they are unconformably covered by molasse type sediments. The fluorite mineralizations are detected in two localities associating with the late orogenic granitic plutons of Gabal Homrit Waggat and Gabal Ineigi, (Fig. 1).

Gabal Homrit Waggat granite, which was deposited at the end of the Pan African orogeny 535 Ma, [18] is located on the eastern side of Gabal Abu Diyab. On the other hand, Gabal Ineigi granite forms a relatively large pluton at the western side of Gabal Abu Diyab, it covers around 300 km² and is characterized by a zonal structure. These two granitic plutons are represented by the coarse-grained biotite muscovite granite of the late orogenic stage. These types of granites had been considered by

[19] to relate to the third phase of the younger granites.

Field relationship indicates that these granites are younger than the medium-grained biotite granite, (Fig. 2). Some of these granites are affected by the action of metasomatic alteration of some surrounded minerals as muscovite, biotite, microcline, albitized, silicified granites and apogranites as shown along with the northern parts of Gabal Homrit Waggat, (Fig. 2). On the other hand, these granites are considered as highly fractionated garnet-bearing granites [20]. Economically, they represent the mineralized granites, however, some fluorite veins dissected them. Moreover, [20] mentioned that the Sn-Nb-Ta-W- REES mineralization of Homrit Waggat granites is related to the albite granite (apogranite). These granites cut the metavolcanosedimentary sequence and metagabbro rocks of island arc assemblage, covering an area up to 50 km². Sets of faults cut the Homrit Waggat pluton in a NW-N direction [21] (Fig. 3). It is invaded by quartz veins and few pegmatite pockets of Fe-Mn oxides, as well as fluorite veins up to 2m and 30m long, cut through it, mainly in the NNW direction [22]. The fluorite veins and veinlets are clearly detected at the northern part of the pluton cutting either the apogranite altered zone of the coarse-grained biotite muscovite granite.

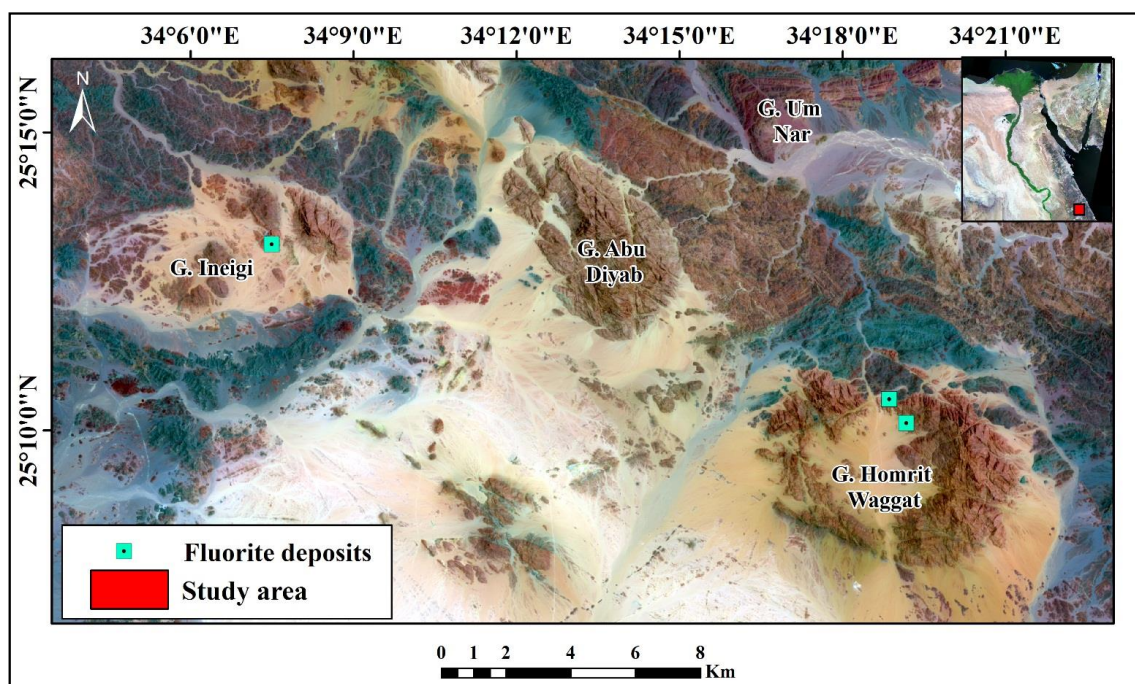


Fig.1. Landsat-8 image (7, 4, 2) in RGB showing the location of the study area.

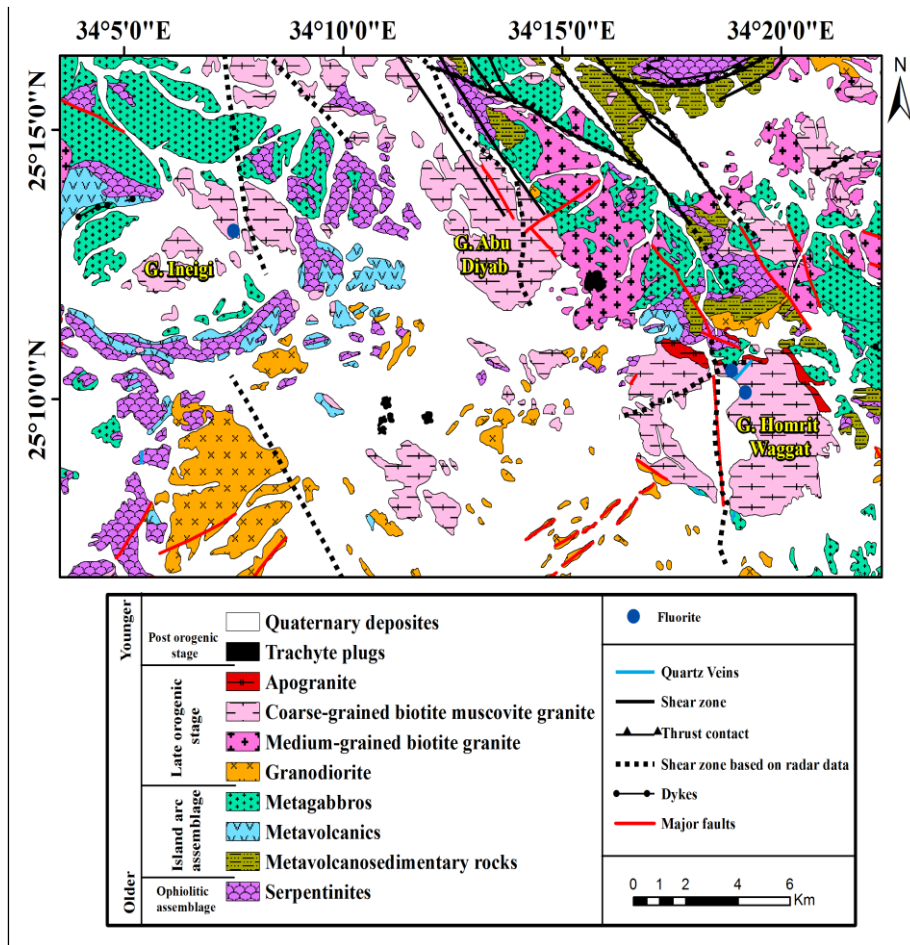


Fig. 2. Geologic map of Gabal Abu Diyab area, Central Eastern Desert, Egypt (modified after [23])

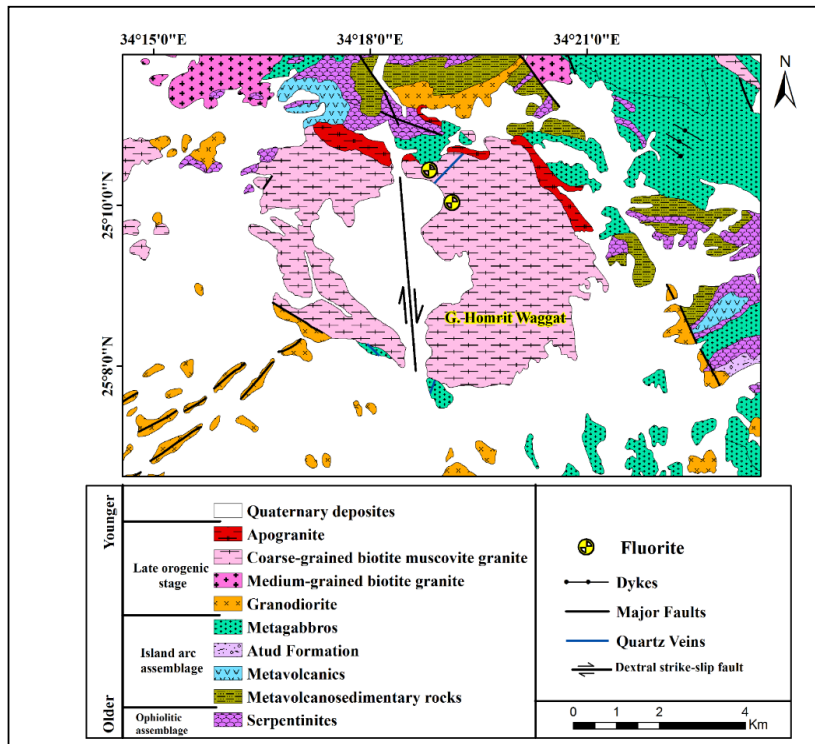


Fig. 3. Geologic map of Gabal Homrit Waggat area showing the lithological rock units with fluorite deposits (modified after [23])

The fluorite veins are associated with quartz and pegmatite veins (Fig. 4A) indicating that they have been related to the formation of the metasomatic processes affecting the area (Fig. 3). The granitic pluton of Gabal Ineigi is also associated with some pegmatites, as well as fluorite veins. The pluton intrudes the serpentinites and metagabbros (Fig. 5). It is revealed that the fluorite mineralizations are often associated with quartz veins, however, pure fluorite veins are rare, [20]. These veins are fillers for open large and small cracks that have formed along with fault plans. Fluorite veins are mostly found in the pluton's southern side. Usually, these veins are varying in

thickness from 0.5m to 5m and in length from 20m to over 300m and with trend mainly N 70 E with 88° dip to NW or SE [20]. The fluorite veins have been examined by several authors e.g., [24-29]. [20] considered that the fluorite-quartz veins had been created as filling of fissures and fractures during cooling of plutons which dissecting by some parallel fractures (Fig. 4B), after that, magmatic fluids rich in fluorite from crystallization granitic melt were injected into the fractured zones at moderate temperatures and salinity. Quartz veins with lower temperatures and salinities had developed during the late stages of magmatic fluids.

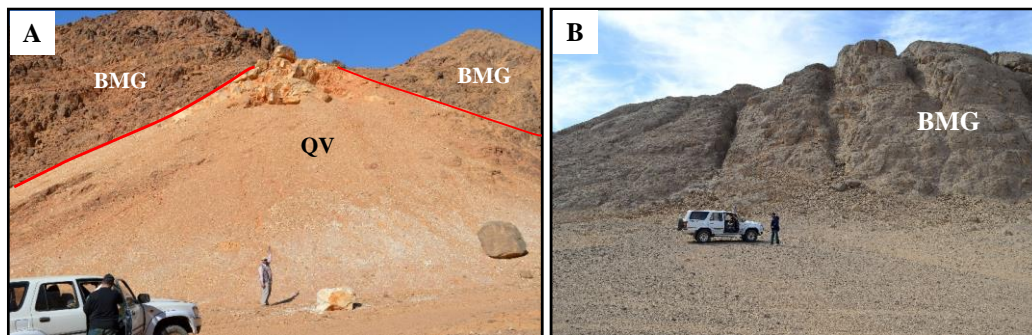


Fig. 4. (A) Photograph showing the quartz vein (QV) cutting the coarse-grained biotite muscovite granite (BMG) of Gabal Homrit Waggat. (B) Photograph showing some parallel deep fractures dissecting the coarse-grained biotite muscovite granite of Gabal Ineigi.

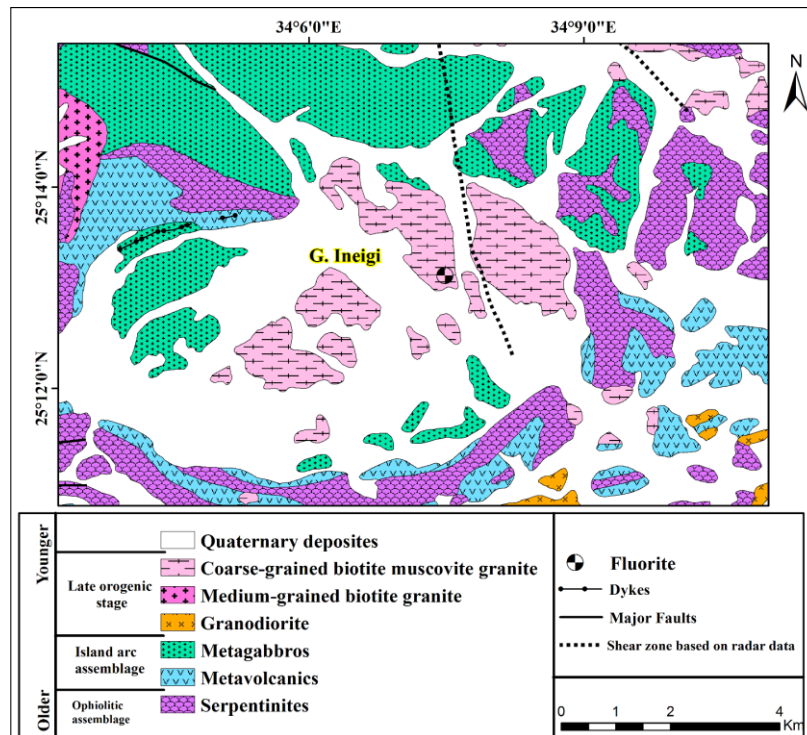


Fig. 5. Geologic map of Gabal Ineigi area showing the lithological rock units with fluorite deposits (modified after [23]).

3. DATA AND METHODS

3.1. Data Characteristics

The Advanced Spaceborne Thermal Emission and Reflection Radiometer (ASTER) level-1B image is multispectral imagery that covering the study area was acquired on February 18, 2007. The ASTER image has 14 bands covers the following ranges: Visible and Near infrared (VNIR) which consist of three bands between 0.52-0.78, shortwave infrared (SWIR) that contains 6 bands between 1.60-2.43 μm within 30 m pixel size and thermal infrared (TIR) which consist of five bands between 8.12-11.65 μm in 90 m pixel size (Table 1). The UTM (Universal Transverse Mercator), Zone N36, related to the WGS-84 datum, is the projection system which used for the ASTER data. The ASTER level-1B image is processed using ENVI 5.3 software and Arc 10.8 from Environmental Systems Research Institute (ESRI) [30].

3.2. Pre-Processing of Remote Sensing Data

The pre-processing steps were applied as the critical procedure needed for minimizing the sensor, solar, atmospheric, topographic effects, and distortion for surface reflectance analysis [31]. The preprocessing steps have a general order in which they should be

performed, otherwise they can significantly impact analysis results [32]. The first step was applying a radiometric calibration for converting the digital numbers (DNs) of each pixel to Top of Atmospheric (TOA) Radiance using the gain and offset values, which are recorded inside the metadata file for images in the metadata file. Following that, the atmospheric correction was performed, which included rescaling and converting the radiance data of optical sensors to surface reflectance data. Hence, the resulting reflectance spectral bands may be calibrated and compared to standard reflectance spectra taken in the lab and the field. [33]. After that, radiometric calibration, layer stacking, and resampling of the spatial resolution were performed on the ASTER sensor's VNIR and SWIR bands. For conducting atmospheric correction and radiance-reflectance conversion in ASTER VNIR–SWIR data, we used the FLAASH (Fast Line-of-sight Atmospheric Analysis of Spectral Hypercube) method using radiometrically calibrated radiance data with the (BIL) format. [34].

3.3. Optical Image based mineral occurrence

Band ratio is an effective image processing method used in remote sensing because it accentuates spectral variations of surface

Table 1: The radiometric characteristics of ASTER data

Sensor	Bands	Spectral Region	Wavelength (μm)	Resolution (m)
ASTER	Band 1	VNIR	0.52–0.60	15
	Band 2		0.63–0.69	
	Band 3		0.78–0.86	
	Band 4	SWIR	1.60–1.70	30
	Band 5		2.145–2.185	
	Band 6		2.185–2.225	
	Band 7		2.235–2.285	
	Band 8		2.295–2.365	
	Band 9		2.360–2.430	
	Band 10	TIR	8.125–8.475	90
	Band 11		8.475–8.825	
	Band 12		8.925–9.275	
	Band 13		10.25–10.95	
	Band 14		10.95–11.65	

materials and exposes anomalies, while suppresses other information like scene illumination variances. [4]. Ratio images are mathematical adjustments for improvements obtained by dividing DN values in one spectral band by corresponding values in another. Consequently, this technique was utilized in the present study to enhance the discrimination between rock units since ratioed images describe the variations in the slopes of the spectral reflectance curves between two bands included, regardless of the absolute reflectance values seen in the bands [35]. Band rationing was applied on multispectral bands of both ASTER and OLI sensors for detecting the mineral occurrence in the study area.

4. RESULTS AND DISCUSSIONS

ASTER band ratio $[(b8/b6) * (b5/b3)]$ is used in this study and proved to be an effective tool in detecting the occurrence of fluorite minerals in the study area. The spectral library of the United States Geological Survey (USGS) contains reference spectra for around 200 minerals [36]. In the present study, the USGS reference spectral libraries are used as a reference spectrum of the fluorite mineral. The wavelengths range of the fluorite minerals is between 0.35 to 2.97 μm with sample ID (WS416) of USGS spectral libraries. By dividing one reflectance band by another, this

band ratio has been extracted by tracing the fluorite mineral curves to identify the maximum and minimum reflectance. Fluorite minerals tend to have strong absorption features in VNIR (0.4 to 1.1 μm), coinciding with band 3 of ASTER, and high reflectance in SWIR (2.145 μm to 2.36 μm), coinciding with bands 5, 6 and 8 of ASTER based on the USGS spectral profiles of the fluorite mineral (Fig. 6). Hence, bands 3, 5, 6, and 8 of ASTER were used for calculating Fluorite minerals Index (FI). A new ASTER band ratio image that represented as fluorite index $[(b8/b6)*(b5/b3)]$ has been created to extract the fluorite mineral with yellow pixel color (Fig. 7) using density slice range about (0.0850) by applying $[\text{Mean} + 3 * \text{St dev}]$ formula. This index (FI) has almost identified the fluorite deposits at Gabal Homrit Waggat and Gabal Ineigi granites. The field study reveals that the fluorite mineral occurrence at Gabal Homrit Waggat is associated with quartz veins (Fig. 4A). The structure field study proves that the intersection of Um Nar shear zone (Najd Fault System, NFS) are the favorable localities of structural controlled mineralization of rare metals bearing apogranites and fluorite at Gabal Homrit Waggat and Gabal Ineigi granites. The action of this shear zone is also observed within the banded iron formation with clear displacement along Um Nar plunging anticline.

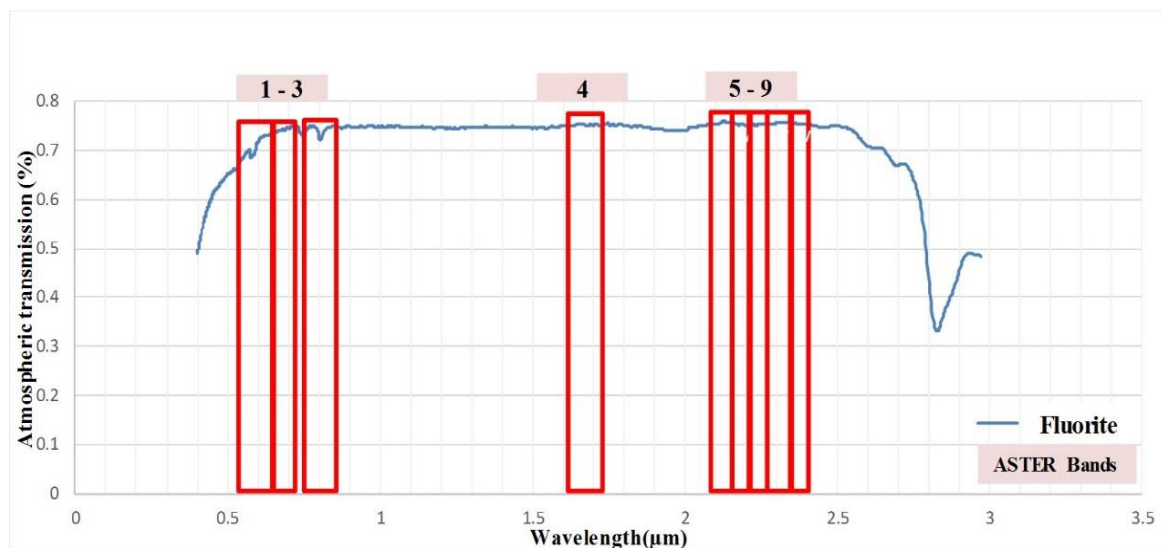


Fig. 6. Plots of fluorite mineral's continuum and continuum removed spectrum

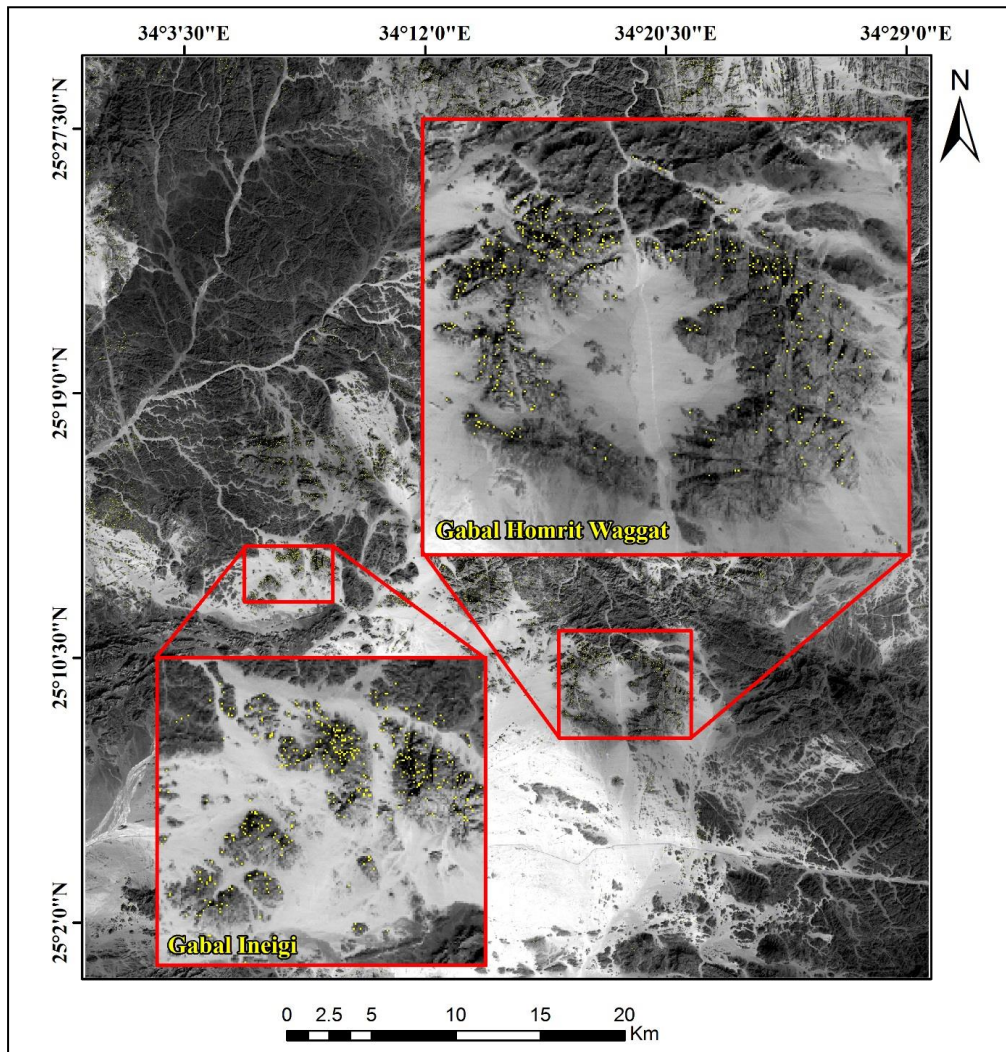


Fig. 7. ASTER band ratio image $[(b8/b6) * (b5/b3)]$ overlaying on ASTER (band1) showing the fluorite mineral with yellow pixel color at G. Homrit Waggat and G. Ineigi.

CONCLUSION

In this paper, a multispectral dataset was used to define the localities of the fluorite mineral around the Abu Diyab area. The fluorite mineral's continuum and continuum removed spectra from the USGS spectral libraries have been studied and analyzed to get a new fluorite Index. The fluorite mineral spectra have sample ID (WS416) and their wavelength ranges between 0.35 to 2.97 μm . By tracking the fluorite mineral curves to find out the maximum and minimum reflectance to extract the band ratio by dividing one reflectance band by another. The new band ratio $[(b8/b6) * (b5/b3)]$ is created to separate the fluorite mineral in ASTER image with yellow color pixels by density slice range about

(0.0850) according to $[\text{Mean} + 3 * \text{St dev}]$ formula. The results of this study identified two occurrences of fluorite mineralization in the study area in Gabal Homrit Waggat and Gabal Ineigi. The identified locations are consistent with the confirmed fluorite occurrences [17&23] and verified by our field work. The results of this study point out that this FI could be a beneficial tool for the fluorite exploration in similar arid and semi-arid environments.

REFERENCES

- [1] Agar R. Geoscan Airborne Multi-Spectral Scanners as Exploration Tools for Western Australian Diamond and Gold Deposits. *Exploration Geophysics*. 1994;25(3):171-172.
- [2] Sultan M, Arvidson R, Sturchio N. Mapping of serpentinites in the Eastern Desert of Egypt by

- using Landsat thematic mapper data. *Geology*. 1986;14(12):995.
- [3] Oppenheimer C. SABINS, F. F. 1997. *Remote Sensing. Principles and Interpretation*, 3rd ed. xiii + 494 pp. New York: W. H. Freeman & Co. Price £32.95 (hard covers). ISBN 0 7167 2442 1. *Geological Magazine*. 1998;135(1):143-158.
- [4] Sabins F. Remote sensing for mineral exploration. *Ore Geology Reviews*. 1999;14(3-4):157-183.
- [5] Abdelsalam M, Stern R, Berhane W. Mapping gossans in arid regions with Landsat TM and SIR-C images: the Beddaho Alteration Zone in northern Eritrea. *Journal of African Earth Sciences*. 2000;30(4):903-916.
- [6] Ramadan T, Abdelsalam M, Stern R, Mapping gold-bearing massive sulfide deposits in the Neoproterozoic Allaqi suture, SE Egypt with Landsat TM and SIR-C/X-SAR images. *Journal of Photogrammetric Engineering and Remote Sensing*. 2001;67(2): 491-497.
- [7] Kusky T, Ramadan T. Structural controls on Neoproterozoic mineralization in the South Eastern Desert, Egypt: an integrated field, Landsat TM, and SIR-C/X SAR approach. *Journal of African Earth Sciences*. 2002;35(1):107-121.
- [8] LIU F, WU X, SUN H, GUO Y. Alteration Information Extraction by Applying Synthesis Processing Techniques to Landsat ETM+ Data: Case Study of Zhaoyuan Gold Mines, Shandong Province, China. *Journal of China University of Geosciences*. 2007;18(1):72-76.
- [9] Crósta A, Moore M. Enhancement of Landsat Thematic Mapper imagery for residual soil mapping in SW Minas Gerais State Brazil: a prospecting case history in greenstone belt terrain. 9th Thematic Conference on Remote Sensing for Exploration Geology, Environmental Research Institute of Michigan, Ann Arbor. 1989;1173-1187.
- [10] Loughlin W. Principal component analysis for alteration mapping. *Photogrammetric Engineering and Remote Sensing*. 1991;57(3), 1163-1169.
- [11] Rokos D, Argialas D, Mavrantza R, Seymour K, Vamvoukakis C, Kouli M, Lamera S, Paraskevas H, Karfakis I, Denes G. Structural mapping and analysis for a preliminary investigation of possible gold mineralization by using remote sensing and geochemical techniques in a GIS environment: study area: island of Lesvos, Aegean Sea, Hellas. *Natural Resources Research*. 2000; 9(1), 277-293.
- [12] Ferrier G, White K, Griffiths G, Bryant R. The mapping of hydrothermal alteration zones on the island of Lesvos, Greece using an integrated remote sensing dataset. *International Journal of Remote Sensing*. 2002; 23(2), 341-356.
- [13] Crósta A, De Souza Filho C, Azevedo F, Brodie C. Targeting key alteration minerals in epithermal deposits in Patagonia, Argentina, using ASTER imagery and principal component analysis. *International Journal of Remote Sensing*. 2003;24(21):4233-4240.
- [14] Ninomiya Y, Fu B, Cudahy T. Detecting lithology with Advanced Spaceborne Thermal Emission and Reflection Radiometer (ASTER) multispectral thermal infrared "radiance-at-sensor" data. *Remote Sensing of Environment*. 2005;99(1-2):127-139.
- [15] Gad S, Kusky T. Lithological mapping in the Eastern Desert of Egypt, the Barramiya area, using Landsat thematic mapper (TM). *Journal of African Earth Sciences*. 2006;44(2):196-202.
- [16] Gad S, Kusky T. ASTER spectral ratioing for lithological mapping in the Arabian-Nubian shield, the Neoproterozoic Wadi Kid area, Sinai, Egypt. *Gondwana Research*. 2007;11(3):326-335.
- [17] Shalaby I, Rossman D, Tabarak D, Emam I. *Geologic map of Aswan quadrangle, Egypt*. Egyptian Geological Survey and Mining Authority. 1983.
- [18] El-Manharawy M. *Geochronological investigations of some basement rocks in the Central Eastern Desert, Egypt, between latitudes 25°-26° N*. Ph.D. dissertation, Cairo University, Cairo, Egypt. 1977:220.
- [19] Sabet A, Tsogoev V, Baburin L, Raid A, Zakhari A, Armanius L. Geologic structure and laws of localization of tantalum mineral zonation at the Nuweibi deposit. *Ann Geol Surv Egypt VI*. 1976; 69(1):119-156.
- [20] Salem I, Abdel-Moneum A, Shazly A, El-Shibiny N. Mineralogy and geochemistry of Gabal El-Ineigi Granite and associated fluorite veins, Central Eastern Desert, Egypt: application of fluid inclusions to fluorite genesis. *Journal of African Earth Sciences*. 2001;32(1):29-45.
- [21] Mohamed F, El-Sayed M. Post-orogenic and anorogenic A-type fluorite-bearing granitoids, Eastern Desert, Egypt: Petrogenetic and geotectonic implications. *Geochemistry*. 2008;68(4):431-450.
- [22] Moghazi A. Magma source and evolution of Late Neoproterozoic granitoids in the Gabal El-Urf area, Eastern Desert, Egypt: geochemical and Sr-Nd isotopic constraints. *Geological Magazine*. 1999;136(3):285-300.

- [23] Abd EL Nabi A, Abd El Karim R, Abu El Leil I, Awad G, Babourin L, Bagadaev E, Bessonenko V, El-Badri H, El Kadi M, Gabra S, Khalaf I, Kosa M, Kouznetsov D, Kouznetsov V, Semyonov V, Spiridenov V, Vitkovsky I, Zalata A, Zhukov M. Geologic map of the basement rocks of Jabal Um Ghayj quadrangle, Egypt. 1989.
- [24] Moustafa G, Kabesh M, Abdalla A. Geology of Gebel El-Ineigi District. Geological Survey, Cairo, Egypt. 1954; 40(1):39-43.
- [25] Moharram O, El-Ramly M, Amer A, Gachechiladze D, Ivanov S. Studies on some mineral deposits of Egypt. Annals Egyptian Geological Survey. 1970: 260.
- [26] Heikal M. Petrographical and petrochemical studies of G. El-Ineigi granitic rocks. Ph.D. dissertation, Faculty of Science, Cairo University, Egypt. 1973: 176.
- [27] Fafous B, Awad N. Mineralization and petrochemical features of El-Ineigi fluorite deposit, Eastern Desert, Egypt. Bulletin National Research Center Egypt. 1985; 10(2):299-313.
- [28] Yonan A. Mineralogical, petrochemical and geochemical studies on granites hosting fluorite mineralization in the Eastern Desert of Egypt. Ph.D. dissertation, Ain Shams University, Cairo, Egypt. 1990:246.
- [29] El-Shibiny N. Petrological and geochemical studies on the mineralization in selected granitic plutons in the Idfu-Mersa Alam District, Eastern Desert, Egypt. Ph.D. dissertation, Tanta University, Tanta, Egypt. 1995:376.
- [30] Plimmer F. Land Administration for Sustainable Development 2011 Han Williamson, Stig Enemark, Jude Wallace and Abbas Rajabifard. Land Administration for Sustainable Development. Redlands, CA: ESRI Press Academic, ISBN: 978-1-58948-041-4. Property Management. 2011;29(3):324-324.
- [31] Young N, Anderson R, Chignell S, Vorster A, Lawrence R, Evangelista P. A survival guide to Landsat preprocessing. Ecology. 2017;98(4):920-932.
- [32] Sundaresan S, Fischhoff I, Dushoff J, Rubenstein D. Network metrics reveal differences in social organization between two fission-fusion species, Grevy's zebra and onager. Oecologia. 2006;151(1):140-149.
- [33] Zoheir B, Emam A, Abd El-Wahed M, Soliman N. Gold endowment in the evolution of the Allaqi-Heiani suture, Egypt: A synthesis of geological, structural, and space-borne imagery data. Ore Geology Reviews. 2019; 110:102938.
- [34] Cooley T, Anderson G, Felde G, Hoke M, Ratkowski A, Chetwynd J, Gardner J, Adler-Golden S, Matthew M, Berk A, Bernstein L, Acharya P, Miller D, Lewis P. FLAASH, a MODTRAN4-based atmospheric correction algorithm, its application and validation. IEEE International Geoscience and Remote Sensing Symposium. 2002; 3(1):1414-1418.
- [35] Denniss A. T. M. Lillesand, & R. W. Kiefer, 1994. Remote Sensing and Image Interpretation, 3rd ed. xvi + 750 pp. New York, Chichester, Brisbane, Toronto, Singapore: John Wiley & Sons. Price £67.00 (hard covers), £19.95 (paperback). ISBN 0 471 30575 8 (pb). Geological Magazine. 1995;132(2):248-249.
- [36] Clark R, Swayze G, Wise R, Livo E, Hoefen T, Kokaly R, Sutley S. USGS digital spectral library splib06a: U.S. Geological Survey, Digital Data Series. 2007; 231.

مؤشر معادن جديد لاستكشاف الفلوريت باستخدام بيانات الأستر لمنطقة جبل أبو دياب ، وسط الصحراء الشرقية ، مصر

محمود حافظ⁽¹⁾، إبراهيم أبو الليل⁽¹⁾، نهال سليمان⁽²⁾، مصطفى أبو بكر⁽¹⁾

1. قسم الجيولوجيا - كلية العلوم - جامعة الأزهر - القاهرة - مصر
2. قسم الجيولوجيا - الهيئة القومية للاستشعار من البعد وعلوم الفضاء - القاهرة - مصر

المخلص:

الاستشعار عن بعد يلعب دور هام جدا في استكشاف المعادن. أحد تطبيقاته المؤكدة هو استخراج وتحديد تواجد المعادن في المناطق شبه القاحلة إلى القاحلة. تم استخدام صور مقياس الإشعاع الانعكاسي والانبعث الحراري المتقدم في الفضاء الأستر (ASTER) مع تقنية معالجة نسبة النطاق للكشف عن وجود معدن الفلوريت حول منطقة جبل أبو دياب ، وسط الصحراء الشرقية ، مصر. يمكن اعتبار نسبة النطاق المقترحة المشتقة من صور الأستر $[(b5 / b3) * (b8 / b6)]$ لتمثيل مؤشر الفلوريت الجديد (FI). تم استخدام مكتبة هيئة المساحة الامريكية (USGS Spectral) لطيف المعادن لاستخراج المؤشر الجديد والتحقق من صحته باستخدام الدراسة الميدانية. وفقاً لمؤشر الفلوريت الجديد (FI) جنباً إلى جنب مع الملاحظات الميدانية ، تم تحديد تواجدين لتمعدن الفلوريت في جبل حمريت واجات وجبل عنيجي. تقدم هذه الدراسة مؤشر الفلوريت الجديد المقترح كأداة مفيدة لاستكشاف الفلوريت التي يمكن تطبيقها على طول الدرع العربي النوبي والبيئات القاحلة وشبه القاحلة المماثلة.